Version of Record: https://www.sciencedirect.com/science/article/pii/S0254058418304553
Manuscript_5610fd1143b21f260ad28172892e23d6

Investigation of plastic deformation modes in $Al_{0.1}CoCrFeNi$ high entropy alloy

D. Choudhuri[1,2], M. Komarasamy[1,3], V. Ageh[1,2], and R.S. Mishra[1,2,3]*

[1] Department of Materials Science and Engineering, University of North Texas
Denton, TX-76207, USA
[2]Advanced Materials and Manufacturing Processes Institute, University of North Texas
Denton, TX-76207, USA
[3]Center for Friction Stir Processing, University of North Texas
Denton, TX-76207, USA

* Corresponding author: Rajiv.Mishra@unt.edu

Abstract

Mechanisms contributing to the plastic deformation of coarse grained (CG, average grain diameter 1-2 mm), and friction-stir-processed fine grained (FG, 0.3-14 µm) *fcc* $Al_{0.1}CoCrFeNi$ high entropy alloy was investigated. In the grain interiors of CG, deformation primarily occurred via planar slip of undissociated ½ <011> dislocations on parallel (111) planes. Stacking faults were also detected, and they appeared to have contributed to the formation of parallel (111) slip-bands. In comparison, the deformed FG microstructure was dominated by dislocation cell-like structures, which suggested that proximity to the grain-boundaries, unlike CG, have substantially influenced dislocation arrangements. Interestingly, nanoscale (~2 nm thick) deformation twins were unambiguously observed in both deformed FG and CG microstructures, and that such twins did not emanate from grain boundaries. These twins invariably comprised of two variants, which lay on two different (111) habit planes oriented by ~70˚ from each other. The formation of such two-variant deformation twinning provides an additional plastic deformation mode and is expected to improve the work hardening of $Al_{0.1}CoCrFeNi$ high entropy alloy.

Keywords: High Entropy alloys; Deformation; TEM; Twinning

Highlights:

1. Deformation mechanisms in a coarse and fine grained *fcc* HEA was investigated.
2. Intragranular nano-scale twinning on conjugate {111} were noted in both cases.
3. {111}<110> planar slip-bands dominated CG, while FG had cells-like structures.

1. Introduction

High entropy alloys (HEAs) are promising candidates for structural applications due to their excellent strength-ductility combination and fracture toughness [1]. Microstructures of HEAs can vary from being a single phase solid solutions to those containing primarily ordered intermetallic compounds [1-4]. However, deformation behavior of single phase HEAs have received the most attention due to the simplicity of the microstructure [5-10]. Notably, single *fcc* phase CoCrFeNiMn (a classical solid solution HEA) was extensively investigated for ascertaining the underlying micromechanisms of plastic deformation in HEAs using transmission electron microscopy (TEM). These studies involved relating quasistatic deformation behavior to dislocation arrangements [5], and deformation twinning [6]. Furthermore, such post mortem deformation studies were also complimented with in-situ TEM testing under a transmission electron microscope [7]. Thus, the collective body of work indicates that, under quasistatic conditions, CoCrFeNiMn deforms by planar slip on the (111) planes, partly mediated by stacking fault formation, and deformation twinning [5-7].

Interestingly, such detailed TEM investigation is limited on Al containing HEAs like $Al_xCoCrFeNi$ (x=0.1-0.3), which exist as stable single phase *fcc* solid solutions at room temperature [1,8-11]. Among them, deformation behavior of both coarse and fine grained $Al_{0.1}CoCrFeNi$ have been examined in little more detail than $Al_{0.3}CoCrFeNi$ [11]. By comparing the mechanical responses of coarse and friction stir processed fine grained specimens, Kumar et al.[8] quantified strengthening contributions from solid solution strengthening and Hall-Petch. Effect of deformation twinning on strain-hardenability of $Al_{0.1}CoCrFeNi$ was investigated by both Jang et al. [9] and Komarasamy et al. [10]. By examining deformation features in a coarse and fine grained recrystallized specimen Jang et al. [9] demonstrated that twinning activity is

limited by reducing grain size, and that twins emanate from grain boundaries. Intriguingly, Komarasamy et al. suggested that significantly finer scale twins also form within grain interiors (or intragranular twinning); away from the grain boundary [10]. Furthermore, recent *in situ* TEM observations in CoCrFeNiMn revealed that intragranular nano-scale deformation twins form within the *fcc* matrix near the crack-tips [7]. Based on these studies by Zhang et al.[7], it is plausible that similar intragranular nano-scale twins may form in $Al_{0.1}$CoCrFeNi; as suggested by Komarasamy et al.[10]. To probe this aspect, a detailed TEM characterization of deformation features was carried out in quasistatically tested tensile specimens with coarse and fine grained microstructures.

Therefore, the purpose of this work is to determine various micro-mechanisms contributing to the plastic deformation of $Al_{0.1}$CoCrFeNi HEA. Implicitly, these results will allow us to extract commonalities with CoCrFeNiMn deformation behavior and, from a broader perspective, place plastic deformation of single phase *fcc* HEAs under an unifying umbrella.

2. Materials and Methods

HEA of composition $Al_{0.1}$CoCrFeNi was obtained from Sophisticated Alloys Inc. The HEA was vacuum induction melted and cast (referred to as-received). The rectangular plates cut from the as-received blocks were subsequently subjected to friction stir processing (FSP), and the details of the processing parameters is provided elsewhere [8,10]. Mini-tensile dog-bones were cut from as-received and FSP specimens with nominal gauge length, width and thickness as 2, 1.25 and 0.6 mm, respectively (inset in Figure 1(a)). These min-tensile specimens were uniaxially strained to failure at a strain rate of ~10^{-3} s^{-1} at room temperature using a mini-tensile tester

[8,9,13]. Surface manifestation of deformation features were investigated in a FEI NovaNano scanning electron microscope (SEM). The deformed specimens were further examined via transmission electron microscopy (TEM) in FEI Tecnai F20-FEG™ operating at 200 kV. Site-specific TEM foils were extracted from the deformed regions via focused ion beam (FIB) milling using a FEI Nova NanoLab 200™. To ensure that TEM examination of deformation features is performed for uniaxial stress condition, FIB-based TEM foils were plucked from the gauge section, which was at least~0.4-0.5 mm away from the neck of the failed specimens.

3. Results

3.1. Mechanical behavior and surface manifestation of deformation

Past microstructural characterization efforts has shown that the grain sizes of the as-received condition was 1000-2000 μm (henceforth referred to as coarse grained or CG), while the subsequently friction stir processed materials had grain sizes were significantly refined 3-14μm (hereafter, fine grained or FG) [8]. The measured mechanical properties associated with CG and FG microstructures are listed in Table I, and show the expected trend that CG has a lower strength and higher ductility than FG.

Table I. *Summary of mechanical properties.*

Microstructure	**Grain size (μm)***	**Tensile properties**		
		Yield strength (MPa)	**Ultimate tensile test (UTS)**	**Uniform elongation (%)**
Coarse grained (CG)	~1000-2000	160 ± 7	389 ± 42	44 ± 15
Fine grained	~3-14	544 ± 50	730 ± 19	27± 1

(FG)	

*Grain sizes were obtained from Refs 8 and 10

Representative engineering and true stress-strain plots are also shown in Figure 1(a). Figure 1(b) shows the work-hardening rate curves extracted from the true stress-strain plots of CG and FG specimens. The work-hardening curve of FG could be subdivided into three different regimes, i.e. A, B and C, while the CG microstructure only had B and C. Typically, stages A and C are associated with dislocation-slip mediated plasticity, while stage B is determined by the balance of strain-hardening rate and recovery rate [8,10]. The apparent lack of stage A in CG is subject of an ongoing investigation and will not be discussed further. Regardless, two key differences were noted from the work hardening curves of CG and FG: (1) Stage B in case of CG had a positive slope, while FG had a small negative slope, and (2) till the onset of stage C the work-hardening rate of FG is greater than the CG. .

Failed CG and FG tensile specimens were further examined under SEM in order to differentiate their respective deformation behavior. The surface manifestation of deformation features in failed tensile specimens containing CG and FG microstructures are presented in Figures 1(c) and 1(d), respectively. A careful examination of the CG microstructure revealed that slip traces dominated the grain interiors, and they tend to orient primarily along one direction/plane (schematically shown with a solid black line in Figure 1(c)).

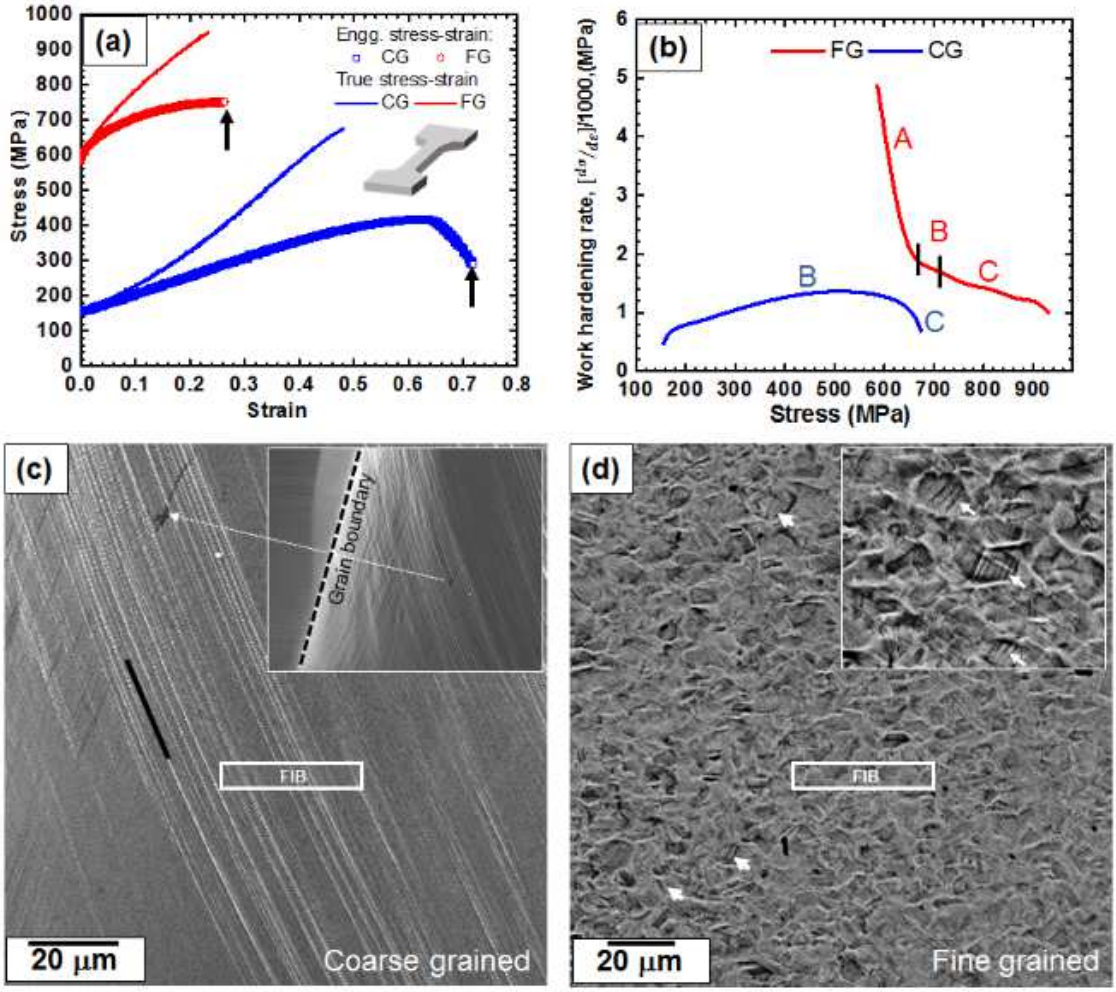

Figure 1. *A comparison of mechanical behavior of coarse and fine grain microstructures using (a) engineering and true stress-strain, and (b) work-hardening rate vs. stress plots. Secondary election microscopy (SEM) showing surface manifestation of deformation in the (c) coarse grained (FG) and (d) fine grained (CG) tensile specimens. The micrographs were recorded after deforming the tensile specimens to failure. Locations of site-specific focused ion beam (FIB) liftouts exacted from deformed regions are also indicated. The insets in (c) and (d) respectively shows the location of the observation though a correlating arrow in the coarse grain microstructure and, deformation features in high magnification inside the fine grained microstructure.*

In other words, the SEM of the CG microstructure suggested that, under uniaxial stress loading, deformation preferentially occurs on (or localized) a primary slip system within the grain interiors. In stark contrast, the FG condition appears to have experienced a relatively

homogeneous deformation (Figure 1(d)). In certain grains parallel linear features (arrows in the inset of Figure 1(d)), which could be a product of either primary slip (comparable to the CG condition), deformation twin formation or annealing twins. These additional features in FG may partially explain its higher work hardening rate than CG. However, the SEM observations along are do not satisfactorily explain the differences in stage B of CG and FG microstructures. Therefore, the deformed CG and FG were examined in detail via TEM.

3.2. Deformation modes in as-received coarse grained microstructure

TEM results showing dislocation structures in the deformed CG specimen are presented in Figure 2. The TEM foil was extracted using FIB, such that multiple slip traces could be sampled in a single foil (Figure 1(b)). The bright-field TEM (BFTEM) images presented in Figure 2 were recorded using two-beam technique, i.e, by exciting **g** = $[\bar{1}\bar{1}1]$, $[1\bar{1}1]$, [200] and $[0\bar{2}2]$ near the [011] zone axis (inset Figure 2(a)). The dotted line in all the BFTEMs indicate the $(\bar{1}\bar{1}1)$ trace and schematically marks the reference for each image. The BFTEMs revealed that the deformation had occurred via planar slip on multiple $(\bar{1}\bar{1}1)$ planes, which is qualitatively comparable to observations reported by Otto et al.[5] in case of deformed CoCrFeNiMn HEA. Note that the dislocation segments which are visible at **g** = $[\bar{1}\bar{1}1]$ and $[1\bar{1}1]$ are invisible in the BFTEMs recorded with **g** = [200] and $[0\bar{2}2]$. Thus, using **g.b = 0** invisibility criterion it was determined that undissociated perfect dislocations with Burgers vector ½ <011> contributes to the planar slip in $Al_{0.1}$CoCrFeNi.

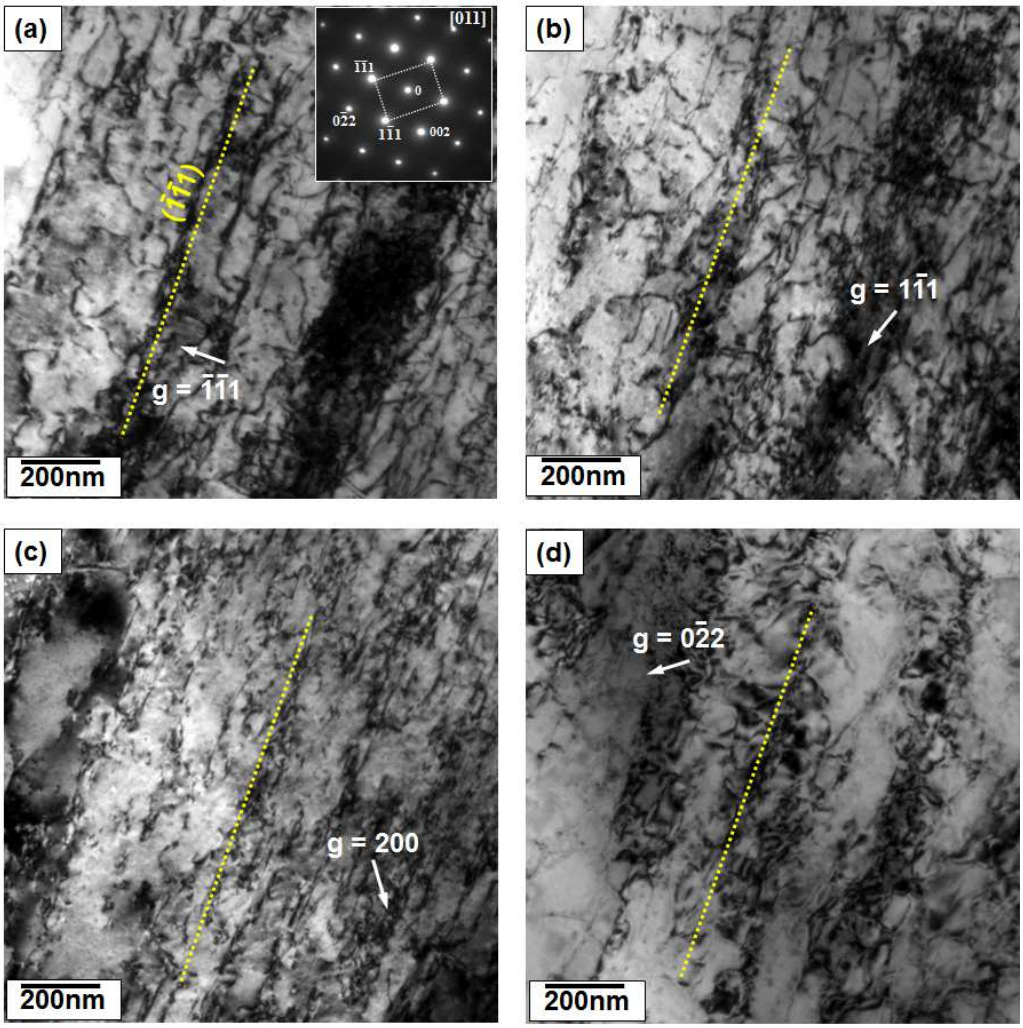

Figure 2. *Identification of dislocation structures in the coarse grained (CG) specimen by using* ***g.b*** *invisibility criterion analysis. Two-beam BFTEMs recorded by exciting* ***g*** *vectors corresponding to (a)* $\mathbf{g} = [\bar{1}\bar{1}1]$*, (b)* $\mathbf{g} = [1\bar{1}1]$*, (c)* $\mathbf{g} = [200]$ *and (d)* $\mathbf{g} = [0\bar{2}2]$*. The dotted lines in the BFTEMs indicate the trace of* $(\bar{1}\bar{1}1)$ *plane and also marks as a reference in each image. Planar slip involving {111} ½ <110> dislocations were noted. Inset in (a) shows the [011] selected area diffraction pattern.*

However, the dislocation structures obtained with two-beam technique alone was insufficient to discern additional features like stacking faults typical seen in *fcc*-based alloys [5]. This is because the deformed microstructure contained very high dislocation number density (~10^{14} – 10^{15} m^{-2}) and their overlapping strain fields (e.g. note the dark-regions in Figure 2(a)) may not

permit identification stacking fault ribbons. Therefore, the deformed CG microstructure was further probed with **g**(**3g**) weak-beam dark field (WBDF). Figure 3(a) shows a WBDF corresponding to the BFTEM shown in Figure 2(a). Regions of interest in the WBDF was further examined at higher magnifications (Figures 2(b) and 2(c)), which revealed the presence of intensity fringes (ellipses in Figure 2(b)) that are typically associated with stacking faults [5]. The crystallographic location of such stacking faults is also schematically shown in Figure 3(d). Even though our results did not unambiguously show the presence of 1/6 <112> Shockley partials, but their presence can be indirectly inferred from the intensity fringes depicting the stacking fault (highlighted in Figure 3(c)).

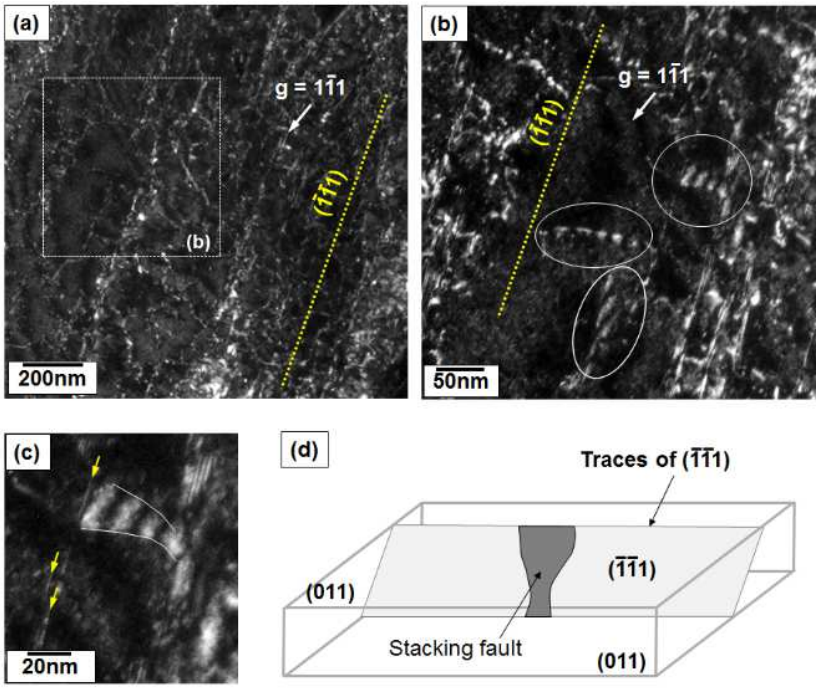

Figure 3. g(3g) *weak beam dark field images showing (a) dislocation structure with* $\mathbf{g} = [1\bar{1}1]$*, and (b) a magnified view of a region selected from (a), which show stacking faults as intensity fringes (marked with ellipses). (c) A magnified view of a staking fault, and (d) crystallography of the fault in the fcc lattice. The arrows in (c) also show very fine scale linear features.*

A careful examination of the regions near the stacking faults also indicated the presence of extremely fine linear segments (marked with arrows in Figure 3(c)). Such linear/straight segments were also visible in the BFTEM shown in Figure 4 (a) (recorded with **g** = [200] along) near some dislocations. These linear segments were further revealed as twin-like features (Figure 4(b)) via tilting experiments away from the [011] zone axis. However, because of their low volume fraction in this FIB liftout, the twin-like features did not manifest themselves as either discrete reflections or streaking in the [011] selected area diffraction pattern (SADP) – e.g. inset in Figure 2(a). Therefore, to confirm the presence of twins, high resolution TEM (HRTEM) imaging was carried out with the electron beam approximately parallel to the [011] zone axis.

The HRTEM presented in Figure 4 (c) shows two prominent features via dotted lines, where the relatively coarse (thickness ~ 1.3 nm, and marked as variant-1) and finer (thickness ~0.5 nm, variant-2) scale entities that lie on the conjugate $(\bar{1}\bar{1}1)$ and $(\bar{1}1\bar{1})$ planes respectively (comparable to twins [5-7,12]). The discreet reflections in the Fast Fourier Transform (FFT) of the HRTEM corresponded to the [011] zone axis (motif indicated with dotted rectangle in the inset of Figure 4(c)), while the frequency streaking corresponding to the features shows a mirror like reflection (bold rectangle) across $(\bar{1}\bar{1}1)$ – as expected from a twin. This FFT primarily contained frequencies generated from the coarser twin lying on $(\bar{1}\bar{1}1)$, while frequencies from fine scale feature was rather diffuse. The thicker variant-1 twin is also indicated with bold fiducial lines in Figure 4(c), which marks the lattice reorientation caused by twinning. Regardless, these results demonstrate that CG specimen has experienced twining during tensile deformation, and that such twins have formed on planes that have experienced dislocation slip inside the grain interiors.

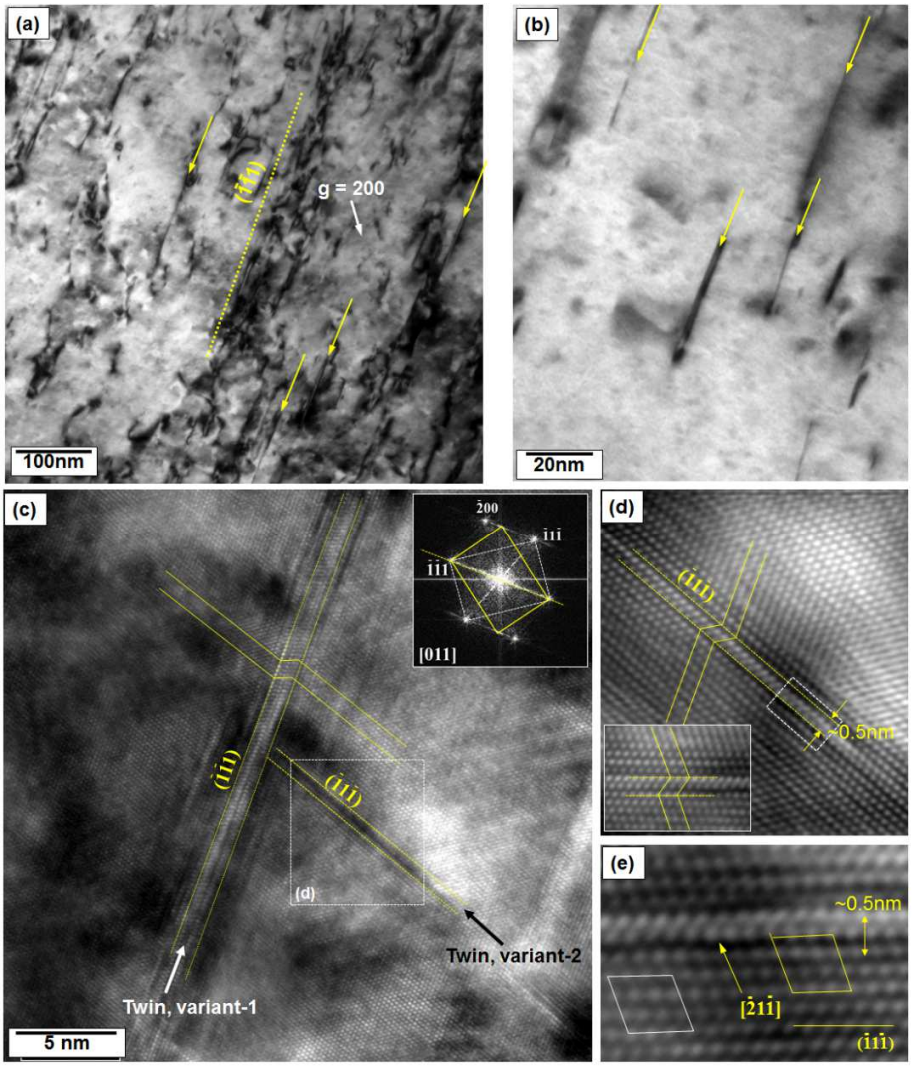

Figure 4. *Deformation twins inside the deformed coarse grained microstructure. BFTEMs showing (a) dislocations near twins (marked with arrows) by imaging under two-beam condition using* $\boldsymbol{g} = [\bar{1}\bar{1}1]$*, and (b) fine scale twins visualized with minimal background contrast by tilting ~12˚away from the [011] zone axis. HRTEM of deformation twins depicting (c) two variants of nanoscale twins (inset shows the corresponding FFT of variant-1), (d) Fourier filtering of the region (dotted rectangle in (c)) comprising variant-2, and (e) a Burgers circuit analysis showing* $1/6[\bar{2}1\bar{1}]$ *partial dislocation near variant-2. Inset in (d) shows the "three-layered" structure inside the finer scale variant-2.*

The finer scale twin-like features in Figure 4(c), marked as variant-2, was further examined in greater detail because its corresponding FFT (inset Figure 4(c)) did not reveal much regarding its structure. Consequently, a portion of that feature (dotted rectangle in Figure 4(a)) was Fourier filtered for structural analysis. Figure 4(d) indicated that regions inside the fine scale feature underwent lattice rotation, comparable to a twin (e.g. variant-1 in Figure 4(d)). A careful examination of those regions (indicated in the bottom right inset of Figure 4(d)), revealed a "three layered" twined structure (marked with horizontal dotted lines in bottom right inset) - originally proposed by Mahajan and Chin [14] as the early stages of twin nucleation. The three layered twin was also suggested to be bound between 1/6<11$\bar{2}$> Shockley partials [14], and their presence was confirmed by performing Burgers circuit analysis on the extreme end of that twin (dotted region in Figure 4(d)). Our analysis revealed a 1/6[$\bar{2}1\bar{1}$] partial dislocation (Figure 4(e)), which is consistent with the theory proposed by Mahajan and Chin [14]. Crucially, the observation of a three-layered twin indicated that variant-2 was at its early stages of development; presumably following its nucleation.

Note that the deformation features seen in the CG specimen were far away (approx. hundreds of microns) from the grain boundary, and that such features were not susceptible to the constraining influences of grain boundaries. However, such constraints may influence the deformation behavior of the FG specimens.

3.3. Deformation modes in friction stir processed fine grained microstructure

Figure 5 shows the cross section of a FIB liftout plucked from the deformed FG microstructure. The TEM foil comprised of three grains (marked as Grain-1, 2, and 3) and an annealing twin. A representative [011] diffraction pattern, recorded from grain 2 (dotted circle in Figure 5(a)), is shown in Figure 5(b). The [011] SADP indicated diffuse streaking (marked with bold and dotted

arrows), which can be associated to extremely fine scale twins (or stacking faults [14]). However, fine-scale twins (marked with bold and dotted arrows) were evident in the high magnification BFTEM presented in Figure 5(c). These fine scale twins lay on the two conjugate {111} planes (bold and dotted lines on top right inset in Figure 5(c)), which could have contributed to diffuse streaking perpendicular $\mathbf{g} = \bar{1}1\bar{1}$ and $11\bar{1}$ in the [011] SADP. In other words, these TEM results suggests that FG microstructure can also deform by forming two variants of twins like the CG microstructure.

Significantly coarser deformation twins were also noted in the FG microstructure; in addition to nanoscale twins. The distribution of such coarse scale twins is depicted via BFTEM in Figure 6(a). Location of the coarser twins in the FIB liftout is indicated with a dotted rectangle in Figure 5(a). The [011] SADP pattern recorded from a coarse twin (dotted circle in Figure 6(a)), and the corresponding dark-field TEM (DFTEM) image in Figure 6(c), further corroborates their presence. These coarse twins formed as parallel plates which are either hundreds of nanometers apart (BFTEM in Figure 6(a)) or separated by barely 10nm (inset in Figure 6(c)). The, latter, closely spaced paired twins was further examined in detail using HRTEM imaging. Figure 6(d) shows the HRTEM along [011] of one such pair (also indicated with BFTEM in the inset), and Figure 6(e) depicts a Fourier filtered image of a region from Figure 6(d) (see dotted rectangle). These results indicated that the *fcc* matrix is sandwiched between the two twins of same variant, and that the interfaces (at the mid-section of these twins) were coherent with the fcc matrix. The coarser twins are well developed (in contrast to the early stages presented in Figures 4(d) and 5(c) for CG and FG, respectively), and the observed coherency are comparable to those reported by Otto et al. and Zhang et al. [5, 7].

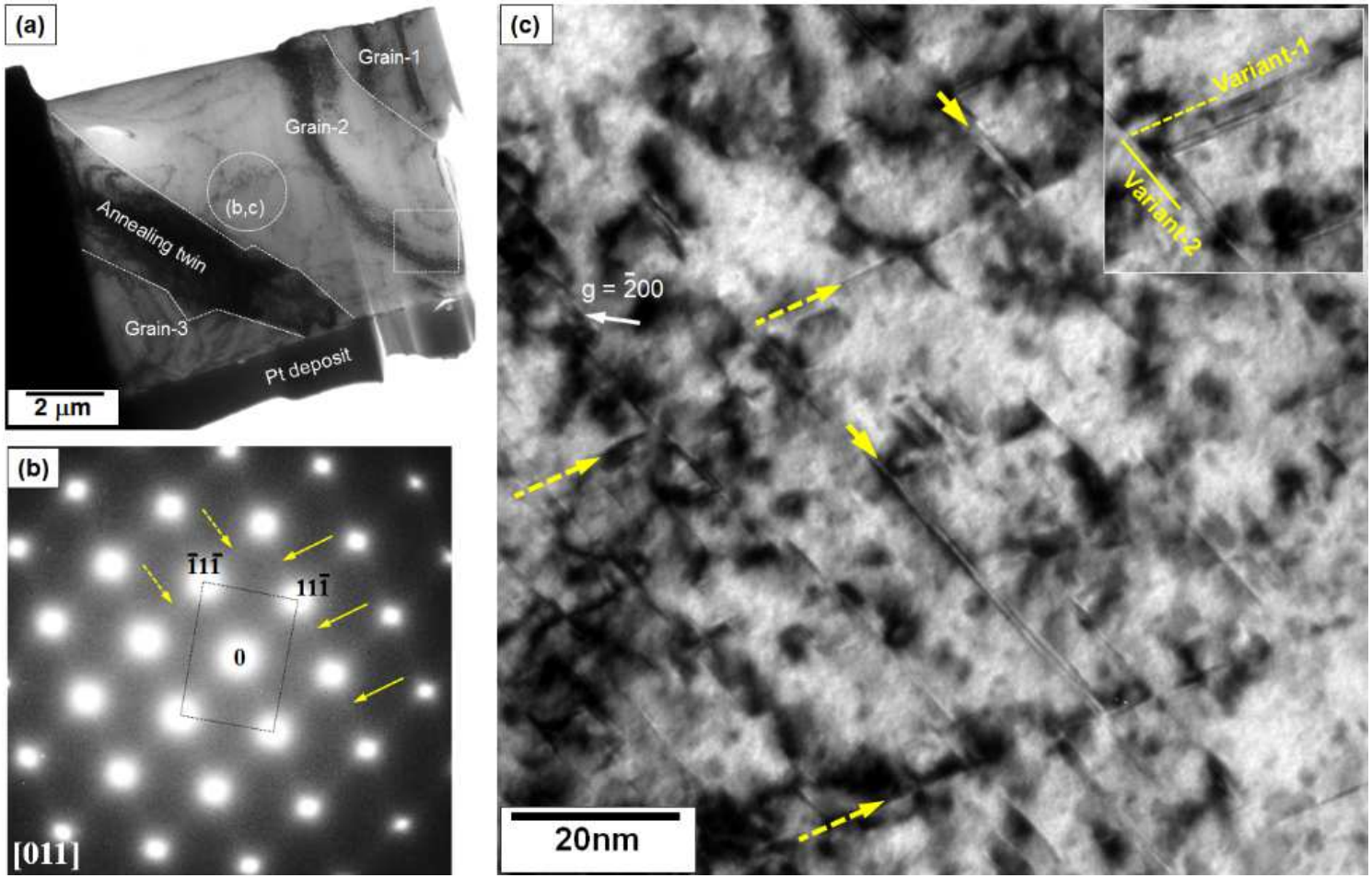

Figure 5. *(a) BFTEM of the FIB liftout extracted from the deformed fine grained microstructure and shows multiple grains and an annealing twin. (b) [011] selected area diffraction pattern (SADP) from the circled region in (a). The SADP shows very diffuse streaking (marked with bold and dotted arrows) corresponding to twining. (c) Corresponding BFTEM which show two variants of nanoscale twins via bold and dotted arrows.*

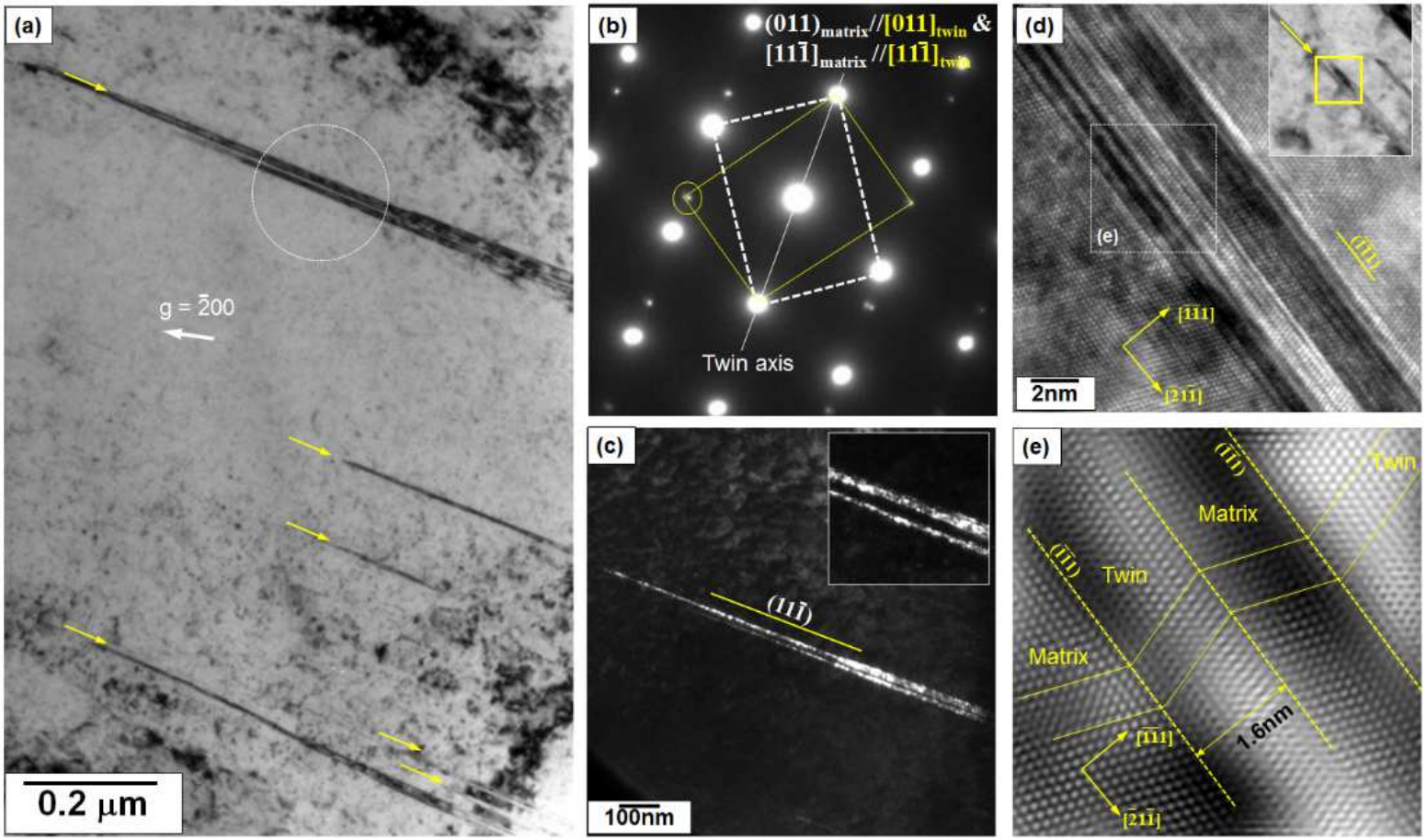

Figure 6. *(a) BFTEM showing distribution of coarser scale twins in the deformed fine grained microstructure. (b) [011] SADP showing discreet reflections from a twin in (a), and (c) the corresponding dark-field TEM image of that twin. (d) HRTEMs showing closely spaced parallel twin,s and (e) Fourier filtering of a chosen region in (d).*

A comparison of size scales between such coarse (in Figure 6) and the substantially finer nanoscale twins (shown in Figure 5) suggested that the coarser twins may have formed earlier during plastic deformation. Therefore, it is very likely that, in addition to dislocation motion, the formation of such coarse twins may have contributed to the plastic deformation of the FG microstructure. It may also be pointed out that the coarser twins could have originated at the grain boundaries [5,9], since their adjoining grain boundary was not captured by the FIB liftout (Figure 5(a)). Accordingly, such coarse twins may also exist at the grain boundaries of the CG microstructure (not show here); as suggested by Otto et. al. [5].

In terms of dislocation structure, the deformed FG microstructure, sampled with the FIB liftout presented in Figure 5(a), had very high dislocation density. As a result, conventional techniques like two-beam and WBDF did not permit identification of dislocation segments, e.g. seen in CG. However, scanning transmission electron microscopy (STEM) in annular dark field (ADF) and annular bright field (ABF) modes presented in Figure 7 allowed us to gain some additional insights. Dislocation arrangements were observed inside the annealing twin and two grains. It may be emphasized that the absence of observable planar slip, which was clearly seen in CG, may be a sampling issue due to the larger number of grains. Nonetheless, these dislocation arrangements seemed to be localized near the high angle grain-grain and twin-grain boundaries. A discussion regarding this matter will be presented in the following section. In addition, the ADF and ABF images also revealed sub-grains boundaries (Figure 7(a),(b) and (d)), which may have formed either during plastic deformation or likely a byproduct of friction stir processing.

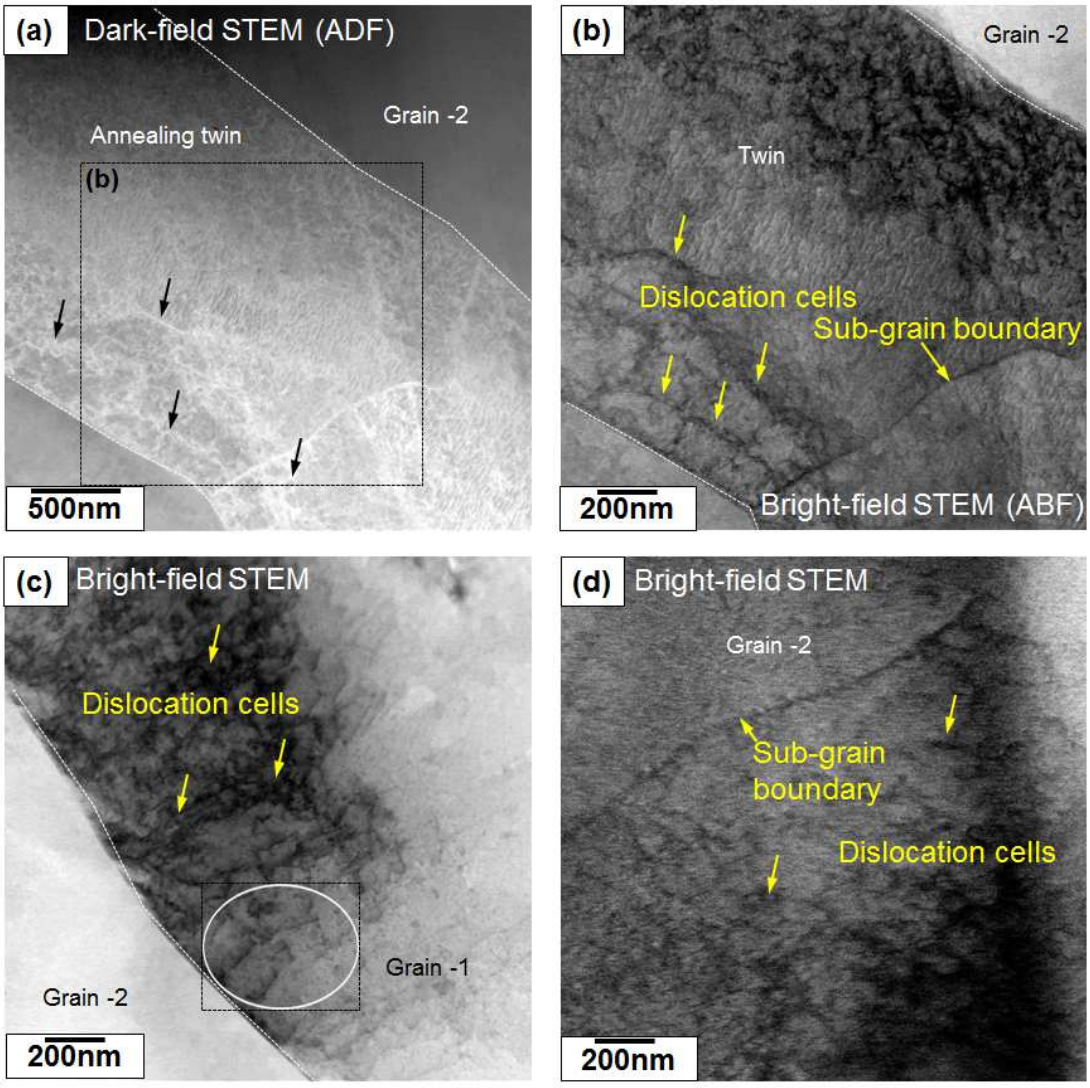

Figure 7. *Scanning transmission electron microscopy (STEM) showing dislocation structures in different grains of the FG specimen: (a) STEM in annular dark-field (ADF) mode showing dislocation structures in grain-3, (b) a region selected from (a) shows the dislocation cells and a subgrain boundary via bright-field STEM or annular bright field (ABF) mode. (c) and (d) ABF STEM showing dislocation cells and subgrain boundary in other grains. In some rare cases, marked with ellipse in (c), individual dislocation segments can also be seen.*

4. Discussion

Our major experimental observation was that two variants of intra-granular nanoscale deformation twins can form in plastically deformed CG (Figure 4) and FG (Figure 5)

microstructures. This observation is important for two reasons. First, twinning on two different habit plane orientations suggests that the additional twinning mode can potentially improve work hardening and fracture toughness of the $Al_{0.1}$CoCrFeNi HEA; simply by providing additional plastic deformation modes during fracture. Second, the nanoscale twins were noted inside the grains and did not emanate from the grain boundaries; unlike typically seen in conventional and high entropy alloys [5-7,12]. This suggests that a different twin-formation mechanism is operative, which may be independent of grain size.

In the CG condition the TEM evidence (Figure 4) suggested that such twins had formed at/near the (111) slip bands. Therefore, it is conceivable that their formation could have been facilitated by the local build-up stress due to dislocation-dislocation interactions with accumulation of plastic strain, which, may have exceeded the threshold/activation stress required for twin nucleation [11]. Such stress may also facilitate the formation of a second variant on a {111} plane oriented ~70˚ from the first twin plane (Figure 4 (c)). Furthermore, the presence of stacking faults (e.g. Figure 3(c)), near such twins could readily supply partial dislocations to sustain twin nucleation and growth. A similar mechanism may have also facilitated their formation in the FG condition. Furthermore, the location of such nanoscale twins near the boundaries of the FG microstructure suggests that build-up of local stresses/strains may also contribute towards deformation twinning.

Irrespective of the mechanisms resulting in two-variant deformation twinning, their formation is not entirely surprising from crystallographic symmetry considerations. The {011} planes have two-fold symmetry, because it contributes to the overall space group symmetry of *fcc* (i.e. F 4/m $\bar{3}$ 2/m) via 2/m. Such two-fold symmetry is also indicated with rectangular motifs in the SADPs (e.g. inset of Figure 2(a) and Figure 5(b)) connecting the two (111) planes and they easily serve

as the habit plane for twinning. Thus, in the absence of any precipitation, the two-variant twin formation will compensate for any "symmetry-breaking" in a given (110) plane [15], while simultaneously satisfying Von Mises criteria involving five deformation modes.

In contrast to deformation twinning, the dislocation arrangements in the failed CG and FG specimens were quite different. The deformation of CG primarily involved planar slip of dissociated ½<110> dislocations on parallel (111) planes (resulting in slip-band formation), while dislocation entanglements comparable to "cell-like" structures were prominently noted in the FG specimen.

Using in-situ TEM studies on CoCrFeMnNi Zhang et al. [7]had reported that the undissociated perfect ½<110> dislocations have a very low mobility, and Otto et al. [5] had indicated that such low mobility occurs due to lattice friction (which they attribute to local ordering) . Mishra et al. [16] have suggested that large lattice distortions present in the multicomponent HEAs may also increase lattice friction and may reduce dislocation mobility by complex variation of dislocation core. Additionally, the observation of stacking faults, confined within the (111) planes (Figure 3), suggested that the 1/6<112> Shockley partials were far apart, which may have limited dislocations from cross-slipping to another plane (similar to the observations by Otto et al. [5]). Thus, a combination of lattice friction and insufficient stress needed to combine Shockley partials (separated by a stacking fault, Figure 3(b)-(c)) may have resulted in localized planar slip in the CG microstructure. Furthermore, since such dislocation mechanism dominated the deformed CG microstructure it is reasonable to assume that planar slip of dislocation primarily contributed to its plastic flow.

Under these circumstances the observation of dislocation "cells" in the FG microstructure is rather perplexing, because such arrangement typically involve cross-slipping mechanism.

Therefore, assuming that FSP did not appreciably change the lattice friction in $Al_{0.1}$CoCrFeNi [16], it appears that sufficiently high local stress were generated during the plastic flow of FG, which overcame the energy barrier required to combine the Shockley partials, and then facilitate their cross-slip to a different (111) plane. These local stresses may have been generated (particularly at the grain boundary regions) simply by the need to maintain continuity between two crystals (grain or annealing twins). Furthermore, study by Kumar et al.[8] on the deformation behavior of $Al_{0.1}$CoCrFeNi HEA revealed that Hall-Petch effect is the main strengthening mechanism in FG microstructures. In other words, the back-stresses generated from the dislocation pileup at the grain boundaries (a necessary requirement for Hall-Petch effect), may further contribute to the local stresses in FG. Regardless, the differences between the dislocation structures in CG and FG provided some insights into the deformation behavior within grain interiors and near boundaries.

Finally, based on the experimental results and the abovementioned discussion, the post-yield strain hardening mechanisms in CG and FG microstructures can be postulated. Recall, from section 3.1 and Figure 1(b), that the primary difference in the work hardening behavior in these conditions was the nature of stage B, i.e. CG had a positive slope while FG had a small negative slope. In addition, the absolute values of strain hardening in stage B of FG are higher (CG ~ 1400MPa and FG ~ 1800MPa). The BFTEM of CG, in Figures 2 (a) and 2(b), indicated several instances of dislocation-line intersections within the narrow slip bands; meaning dislocation-dislocation interactions are one of the contributors to strain hardening. Additionally the formation of nanoscale twins (two variants) on the slip planes suggested that dislocation-twin interactions will also contribute to strain hardening (indicated by the presence of dislocations around the twins in Figures 2, 3, and 4). Thus, restriction in the mean free path for dislocation

movement due to dislocation-dislocation and dislocation-twin interactions are potential causes for strain hardening during the plastic deformation of CG microstructure. Furthermore, it is entirely possible that the number density of deformation twins will continue to increase during plastic flow, which in turn, will increasingly restrict dislocation movement via dislocation-twin interactions – in a "cascading" manner. Therefore, plastic deformation mediated dynamic twin formation and their subsequent influence on dislocation mobility may partly explain the positive slope of stage B in the CG microstructure.

In case of FG, the situation is slightly more complicated due to the constraining influence of high angle boundaries (Figure 5(a)). These boundaries are expected to have at least two effects: first, they can constraint the plastic deformation of the adjoining regions and second, can act as a source or sink for dislocations. The slope of stage B results from the competition between strain hardening (dislocation-dislocation, dislocation-twin interaction) and dislocation annihilation mechanisms, whereas the absolute value of strain hardening represents the extent of hardening mechanism. The small negative slope of FG (Figure 1(b)) suggests that at the higher level of strain hardening is offset by higher rate of dislocation annihilation. Under these circumstances is it suspected that dislocation annihilation is occurs at grain boundaries and via the formation of dislocation cell structures. Further investigations regarding this matter is under progress.

5. Summary

The characterization of deformed $Al_{0.1}CoCrFeNi$ HEA revealed the following similarities and differences between the coarse and fine grained microstructures:

1. Intragranular nano-scale twinning was observed in both coarse and fine grained deformed microstructures. The twins formed as two variants on the two conjugate (111) habit

planes that are oriented ~70˚ to each other. Furthermore, results indicated that these two-variant nanoscale twins formed at the latter stages of plastic deformation. Such deformation twinning mechanisms is expected to improve the fracture toughness by providing additional deformation modes.

2. {111} slip-band formation and 1/6<112> Shockley partials primarily contributed to the plastic flow in the coarse grain microstructure. On the other hand, predominance of dislocation entanglements with cells-like structures in the fine-grained microstructure indicated higher localized strains (compared to the total elongation) during plastic plow; presumably caused by the proximity of high angle grain boundaries.
3. Interactions between the nanoscale-twins and the dislocations caused a positive slope in the stage B of work-hardening in coarse grained microstructure. In case of fine grained microstructure, despite deformation twinning, a negative slope in stage B was noted. It appears that the high-volume fraction of grain boundaries resulted in higher recovery rate during stage B of the fine grained microstructure.

Acknowledgements

The work was performed under a cooperative agreement between the Army Research Laboratory and the University of North Texas (W911NF-16-2-0189). We also acknowledge the Materials Research Facility at the University of North Texas for microscopy facilities.

References

1. Y. Zhang, T.T. Zuo, T. Zhi, M. C. Gao, K. A. Dahmen, P. K. Liaw, Z.P. Lu, Microstructures and properties of high-entropy alloys, Progress in Materials Science 61 (2014) 1-93

2. C.J. Tong, M.R. Chen, J.W. Yeh, S.J. Lin, S.K. Chen, T.T. Shun, S.Y. Chang, Mechanical performance of the AlxCoCrCuFeNi high-entropy alloy system with multiprincipal elements, Metallurgical and Materials Transactions A 36 (2005) 1263-1271.
3. T. Borkar, B. Gwalani, D. Choudhuri, C.V. Mikler, C.J. Yannetta, X. Chen, R.V. Ramanujan, M.J. Styles, M.A. Gibson, R. Banerjee, A combinatorial assessment of Al x CrCuFeNi$_2$ (0< x< 1.5) complex concentrated alloys: Microstructure, microhardness, and magnetic properties, Acta Materialia, 116 (2016) 63-76.
4. D. Choudhuri, B. Gwalani, S. Gorsse, C.V. Mikler, R.V. Ramanujan, M.A. Gibson, R. Banerjee, Change in the primary solidification phase from fcc to bcc-based B2 in high entropy or complex concentrated alloys, Scripta Materialia 127 (2017) 186-190.
5. F. Otto, A. Dlouhý, C. Somsen, H. Bei, G. Eggeler, E. P. George, The influences of temperature and microstructure on the tensile properties of a CoCrFeMnNi high-entropy alloy, Acta Materialia 61 (2013) 5743-5755.
6. G.A. Laplanche, O.M. Kostka, G. Horst, G. Eggeler, E. P. George, Microstructure evolution and critical stress for twinning in the CrMnFeCoNi high-entropy alloy, Acta Materialia 118 (2016) 152-163.
7. Z. Zhang, M. M. Mao, J. Wang, B. Gludovatz, Z. Zhang, S. X. Mao, E. P. George, Q. Yu, R. O. Ritchie, Nanoscale origins of the damage tolerance of the high-entropy alloy CrMnFeCoNi, Nature Communications 6 (2015) 10143.
8. N. Kumar, M. Komarasamy, P. Nelaturu, Z. Tang, P.K. Liaw, R.S. Mishra, Friction stir processing of a high entropy alloy Al$_{0.1}$CoCrFeNi, JOM 67 (2015) 1007-1013.
9. S. W Wu, G. Wang, J. Yi, Y. D. Jia, I. Hussain, Q.J. Zhai, P.K. Liaw, Strong grain-size effect on deformation twinning of an Al$_{0.1}$CoCrFeNi high-entropy alloy, Materials Research Letters 5(2016) 1-8.
10. M. Komarasamy, N. Kumar, Z. Tang, R.S. Mishra, P.K. Liaw, Effect of microstructure on the deformation mechanism of friction stir-processed Al$_{0.1}$CoCrFeNi high entropy alloy, Materials Research Letters 3 (2015) 30-34.
11. Z. Li, S. Zhao, H. Diao, P.K. Liaw, M.A. Meyers, High-velocity deformation of Al$_{0.3}$CoCrFeNi high-entropy alloy: Remarkable resistance to shear failure, Scientific Reports, 7 (2017) 42742.

12. M.A. Meyers, O. Vöhringer, V.A. Lubarda, The onset of twinning in metals: a constitutive description, Acta Materialia 49 (2001) 4025-4039.
13. N. Kumar, D. Choudhuri, R. Banerjee, R. S. Mishra, Strength and ductility optimization of Mg–Y–Nd–Zr alloy by microstructural design, International Journal of Plasticity 68 (2015) 77-97.
14. S. Mahajan, and G.Y. Chin, Formation of deformation twins in fcc crystals." Acta Metallurgica, 21 (1973) 1353-1363.
15. Y. Gao, R. Shi, J.F. Nie, S.A. Dregia, Y. Wang, Group theory description of transformation pathway degeneracy in structural phase transformations, Acta Materialia, 109(2016) 353-363.
16. R.S. Mishra, N. Kumar M. Komarasamy, Lattice strain framework for plastic deformation in complex concentrated alloys including high entropy alloys, Materials Science and Technology 31 (2015) 1259-1263.

Coarse grained microstructure

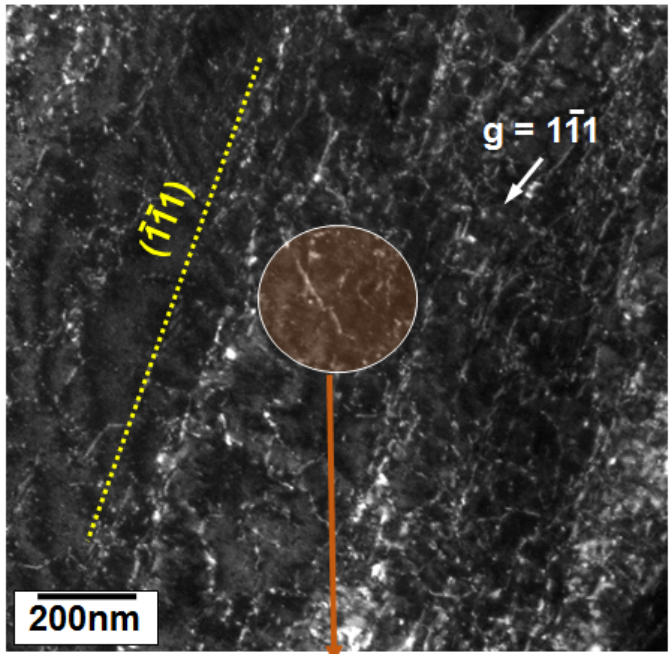

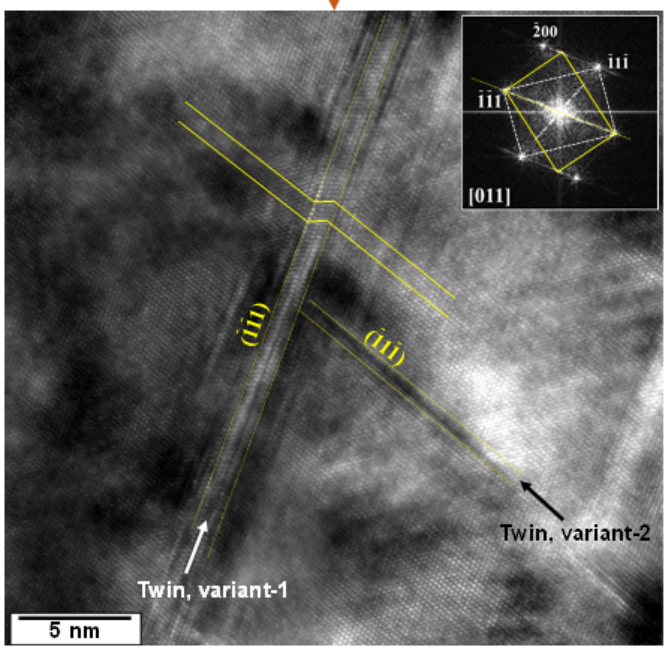

Fine grained microstructure